Continuous Matrix Product States for Quantum Fields: An Energy Minimization Algorithm

Martin Ganahl,* Julián Rincón, and Guifre Vidal
Perimeter Institute for Theoretical Physics, 31 Caroline Street North, Waterloo, Ontario N2L 2Y5, Canada
(Received 16 November 2016; published 2 June 2017)

The generalization of matrix product states (MPS) to continuous systems, as proposed in the breakthrough Letter of Verstraete and Cirac [Phys. Rev. Lett. **104**, 190405 (2010).], provides a powerful variational ansatz for the ground state of strongly interacting quantum field theories in one spatial dimension. A continuous MPS (cMPS) approximation to the ground state can be obtained by simulating a Euclidean time evolution. In this Letter we propose a cMPS optimization algorithm based instead on energy minimization by gradient methods and demonstrate its performance by applying it to the Lieb-Liniger model (an integrable model of an interacting bosonic field) directly in the thermodynamic limit. We observe a very significant computational speed-up, of more than 2 orders of magnitude, with respect to simulating a Euclidean time evolution. As a result, a much larger cMPS bond dimension D can be reached (e.g., $D = 256$ with moderate computational resources), thus helping unlock the full potential of the cMPS representation for ground state studies.

DOI: 10.1103/PhysRevLett.118.220402

Over the past 25 years, progress in our understanding of quantum spin chains and other strongly interacting quantum many-body systems in one spatial dimension has been dominated by a variational ansatz: the matrix product state (MPS) [1–4]. The wave function $|\Psi\rangle$ of a quantum spin chain made of N spin-1/2 degrees of freedom depends on 2^N complex parameters $\Psi_{i_1\ldots i_N}$,

$$|\Psi\rangle = \sum_{i_1=0}^{1}\sum_{i_2=0}^{1}\cdots\sum_{i_N=0}^{1}\Psi_{i_1 i_2\ldots i_N}|i_1 i_2\ldots i_N\rangle. \tag{1}$$

Accordingly, an exact numerical simulation has a computational cost that grows exponentially with the size N of the chain. In a MPS, the 2^N coefficients are expressed in terms of the trace of a product of matrices. For instance, in a translation invariant system, the MPS reads

$$\Psi_{i_1 i_2\ldots i_N} = \mathrm{tr}[A^{i_1}A^{i_2}\ldots A^{i_N}], \tag{2}$$

where A^0 and A^1 are $D\times D$ complex matrices. Thus, the state $|\Psi\rangle$ of N spins is specified by just $O(D^2)$ variational parameters, allowing for the study of arbitrarily large, even infinite, systems [5,6].

A generic state of the spin chain cannot be expressed as a MPS, because the bond dimension D limits how entangled $|\Psi\rangle$ can be. However, ground states of local Hamiltonians happen to be weakly entangled (e.g., they obey an entanglement area law [7,8]) in a way that allows for an accurate approximation by a MPS. Given a Hamiltonian H, White's revolutionary density matrix renormalization group (DMRG) [2,9] algorithm provided the first systematic way of obtaining a ground state MPS approximation by minimizing the energy; see also Ref. [9]. Subsequently, Refs. [10,11] proposed an algorithm to simulate time evolution with a MPS, which in Euclidean time also produces a ground state approximation; see also Refs. [12–14]. An improved formulation of the time evolution simulation by MPS was obtained in terms of the time-dependent variational principle (TDVP) [15].

The continuous version of a MPS (cMPS), introduced by Verstraete and Cirac [16,17], has the potential of duplicating, in the context of quantum field theories in the continuum, the enormous success of the MPS on the lattice. A cMPS expresses the wave function $|\Psi\rangle$ of a quantum field on a circle of radius L as a path ordered exponential $\mathcal{P}e$ of the fields that define the theory. For a bosonic, translation invariant system, it reads

$$|\Psi\rangle = \mathrm{tr}[\mathcal{P}e^{\int_0^L dx Q\otimes\mathbb{1}+R\otimes\psi^\dagger(x)}]|\Omega\rangle, \tag{3}$$

where $\psi^\dagger(x)$ is the bosonic field creation operator,

$$[\psi(x),\psi(y)] = 0, \qquad [\psi(x),\psi(y)^\dagger] = \delta(x-y), \tag{4}$$

$|\Omega\rangle$ is the empty state, i.e., $\psi(x)|\Omega\rangle = 0$, and Q and R are $D\times D$ complex matrices. Again, the wave function $|\Psi\rangle$ is parametrized by just $O(D^2)$ parameters. A cMPS approximation to the ground state of a continuum Hamiltonian H can then be obtained by simulating a Euclidean time evolution with TDVP adapted to cMPS [15]. While this algorithm and its variations work reasonably well for small D up to $D\sim 50$ [18–21], their performance is poor compared to lattice MPS techniques.

In this Letter we propose an energy minimization algorithm to find a cMPS approximation for ground states, based on gradient descent techniques, and demonstrate its performance with the Lieb-Liniger model in the thermodynamic limit ($L\to\infty$). We also propose a useful cMPS initialization scheme, of interest on its own, based on lattice

MPS algorithms. These proposals result in a very significant computational speed-up with respect to Euclidean time evolution—e.g., converging a cMPS with bond dimension $D = 256$ requires less time than a $D = 64$ computation with TDVP. For simplicity, we consider a single bosonic field. Generalization to a fermionic field and to multiple fields is straightforward.

Continuum limit and central canonical form.—In order to describe the algorithm, we must first adjust the notation in two ways. Firstly, following Ref. [16], we discretize the interval $[0, L)$ in Eq. (3) into a regular lattice made of $N \equiv L/\epsilon$ sites and with intersite spacing ϵ, and produce a MPS with matrices A^0 and A^1 [22] given, in vectorized form, by

$$\begin{pmatrix} A^0 \\ A^1 \end{pmatrix} = \begin{pmatrix} \mathbb{1} + \epsilon Q \\ \sqrt{\epsilon} R \end{pmatrix}, \tag{5}$$

such that the original cMPS is recovered in the limit $\epsilon \to 0$ [16]. Here, A^0 and A^1 corresponds to having 0 or 1 particle at the lattice site. This lattice visualization is useful in order to manipulate the cMPS with regular MPS techniques, provided the latter have a well-defined continuum limit ($\epsilon \to 0$). Secondly, we use the lattice visualization to reexpress the cMPS of an infinite system ($L \to \infty$) in the central canonical form [23], Eq. (7) below. For this purpose, we consider the Schmidt decomposition of $|\Psi\rangle$ according to a left-right partition of the resulting infinite lattice [24],

$$|\Psi\rangle = \sum_{\alpha=1}^{D} \lambda_\alpha |\Psi_{l,\alpha}\rangle |\Psi_{r,\alpha}\rangle, \qquad \lambda_1 \geq \cdots \geq \lambda_D > 0, \tag{6}$$

and denote by λ a diagonal matrix with the D Schmidt coefficients $\{\lambda_1, \ldots, \lambda_D\}$ in its diagonal. In the central canonical form, the MPS $|\Psi\rangle$ is expressed as the infinite product of (vectorized) matrices:

$$|\Psi\rangle \sim \cdots \lambda^{-1} \begin{pmatrix} A_c^0 \\ A_c^1 \end{pmatrix} \lambda^{-1} \begin{pmatrix} A_c^0 \\ A_c^1 \end{pmatrix} \lambda^{-1} \begin{pmatrix} A_c^0 \\ A_c^1 \end{pmatrix} \lambda^{-1} \cdots. \tag{7}$$

The matrices A_c^0 and A_c^1 are chosen such that

$$\begin{pmatrix} A^0 \\ A^1 \end{pmatrix} \equiv \begin{pmatrix} A_c^0 \\ A_c^1 \end{pmatrix} \lambda^{-1} \quad \text{and} \quad \begin{pmatrix} B^0 \\ B^1 \end{pmatrix} \equiv \lambda^{-1} \begin{pmatrix} A_c^0 \\ A_c^1 \end{pmatrix} \tag{8}$$

are in the left and right canonical form [3]; namely,

$$(A^0)^\dagger A^0 + (A^1)^\dagger A^1 = \mathbb{1}, \tag{9}$$

$$B^0 (B^0)^\dagger + B^1 (B^1)^\dagger = \mathbb{1}. \tag{10}$$

From Eqs. (7) and (8) the standard MPS form Eq. (2) (in the $L \to \infty$ limit) for, e.g., a left normalized MPS is recovered:

$$|\Psi\rangle \sim \cdots \begin{pmatrix} A^0 \\ A^1 \end{pmatrix} \begin{pmatrix} A^0 \\ A^1 \end{pmatrix} \begin{pmatrix} A^0 \\ A^1 \end{pmatrix} \cdots. \tag{11}$$

In the central canonical form, familiar to DMRG and MPS practitioners working with so-called single-site updates, a change in the matrices A_c^0 and A_c^1 on a single site produces an equivalent change in $|\Psi\rangle$, in the sense that the scalar product in the lattice Hilbert space and in the effective one-site Hilbert space are equivalent (they are related by an isometry). This is important when applying gradient methods, because two gradients, calculated in two different gauges of the same state, are in general not related by a gauge transformation and are not equivalent. The importance of the central gauge has been realized early on in DMRG [2] and also time evolution methods [6,11,23,25–27].

Finally, in the continuum limit, the central canonical form is given by [cf. Eqs. (5) and (8)]

$$\begin{pmatrix} A_c^0 \\ A_c^1 \end{pmatrix} = \begin{pmatrix} \lambda + \epsilon Q_c \\ \sqrt{\epsilon} R_c \end{pmatrix}. \tag{12}$$

Gradient descent.—Given a quantum field Hamiltonian H, see, e.g., Eq. (15), our goal is to iteratively optimize the cMPS in such a way that the energy

$$E(\lambda, Q_c, R_c) \equiv \frac{\langle \Psi | H | \Psi \rangle}{\langle \Psi | \Psi \rangle} \tag{13}$$

is minimized. Each iteration updates a triplet $(\lambda^{[n]}, Q_c^{[n]}, R_c^{[n]})$ and is made of two steps. (i) First, keeping λ fixed, we update Q_c and R_c in the direction of steepest descent given by the gradient; namely,

$$\begin{pmatrix} \tilde{Q}^{[n]} \\ \tilde{R}^{[n]} \end{pmatrix} = \begin{pmatrix} Q_c^{[n]} \\ R_c^{[n]} \end{pmatrix} - \alpha_n \begin{pmatrix} \partial E / \partial Q_c^* \\ \partial E / \partial R_c^* \end{pmatrix}, \tag{14}$$

where $\alpha_n > 0$ is some adjustable parameter and * denotes complex conjugation. Crucially, the gradients $\partial E/\partial Q_c^*$ and $\partial E/\partial R_c^*$ can be efficiently computed using standard cMPS contraction techniques. We dynamically choose the largest possible factor α_n by requiring consistency with some simple stability conditions (alternatively, α_n can be determined by a line search). (ii) Then, from $(\lambda^{[n]}, \tilde{Q}^{[n]}, \tilde{R}^{[n]})$ we obtain $(\lambda^{[n+1]}, Q_c^{[n+1]}\ R_c^{[n+1]})$ by bringing the cMPS representation back into the central canonical form. This completes an iteration, which has a cost comparable to one time step in TDVP. We emphasize that all manipulations are implemented directly in the continuum limit, i.e., ϵ is treated as an analytic parameter throughout the optimization, and the $\epsilon \to 0$ limit can be taken exactly due to exact cancellation of all divergencies.

Overall, the proposed energy minimization algorithm proceeds as follows (see Ref. [28] for technical details).

(a) *Initialization.*—An initial triplet of matrices $(\lambda^{[0]}, Q_c^{[0]}, R_c^{[0]})$ is obtained, either from a random initialization or, as in this Letter, through Eq. (12) from a MPS optimized on the lattice.

(b) *Iteration.*—The above update $(\lambda^{[n]}, Q_c^{[n]}, R_c^{[n]}) \mapsto (\lambda^{[n+1]}, Q_c^{[n+1]}, R_c^{[n+1]})$ is iteratively applied until attaining a suitably converged triplet (λ, Q_c, R_c).

(c) *Final output.*—A standard cMPS representation as in Eq. (3) is recovered by transforming the result into (Q, R).

For instance, $(Q, R) = (Q_c\lambda^{-1}, R_c\lambda^{-1})$ as in Eq. (8) for a final cMPS in the left canonical form (see also Ref. [28]).

As usual in such optimization methods, convergence can be accelerated by replacing the gradient descent in Eq. (14) with, e.g., a nonlinear conjugate gradient update, which reuses the gradient computed in previous steps (see Refs. [28,29]).

Example.—To benchmark the above algorithm, we have applied it to obtain a cMPS approximation to the ground state of the Lieb-Liniger model [30,31],

$$H = \int dx \left(\frac{1}{2m} \partial_x \psi^\dagger(x) \partial_x \psi(x) + \mu \psi^\dagger(x) \psi(x) + g \psi^\dagger(x) \psi^\dagger(x) \psi(x) \psi(x) \right), \quad (15)$$

which is of both theoretical and experimental interest and has been realized in several cold-atom experiments [32–37]. This integrable Hamiltonian has a critical, gapless ground state that can be described by Luttinger liquid theory [35] and can be exactly solved by a Bethe ansatz [30,31,38–41].

Figure 1(a) (blue dots) illustrates the fast and robust convergence of the cMPS with the number of iterations of steepest descent, by showing the energy density $E \equiv \langle H \rangle$, particle density $\rho \equiv \langle \psi^\dagger \psi \rangle$, and reduced energy density e,

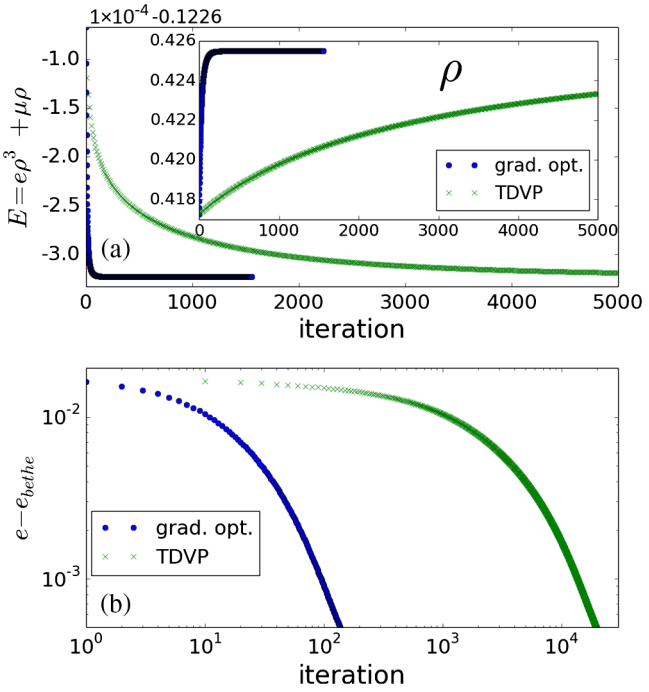

FIG. 1. Convergence of gradient optimization and of TDVP, for $D = 16$ and $(\mu, g, m) = (-0.5, 1.0, 0.5)$. We used $d\tau = 0.01$ as time step for TDVP and $\alpha = 0.01$ for the steepest descent optimization [28]. The time per iteration for either method is 0.2 s. (a) Energy density E (main figure) and particle density ρ (inset) as a function of iteration number. (b) Convergence of reduced energy density e towards the exact value e_{Bethe} as a function of iteration number [43].

$$e \equiv \frac{E - \mu\rho}{\rho^3} = \left\langle \frac{\partial_x \psi^\dagger \partial_x \psi}{2m} + g \psi^\dagger \psi^\dagger \psi \psi \right\rangle \Big/ \langle \psi^\dagger \psi \rangle^3, \quad (16)$$

for bond dimension $D = 16$ and the choice of parameters $(\mu, g, m) = (-0.5, 1.0, 0.5)$. For comparison, we also show the same quantities when the cMPS is optimized instead by a Euclidean time evolution using the TDVP algorithm (green crosses), starting from the same initial state and using values $d\tau = \alpha = 0.01$ for TDVP and for the steepest descent optimization [28], respectively. These values for $d\tau$ are typically used in common TDVP calculations for cMPS [42]. Figure 1(b) then shows the convergence of the energy e to the exact value e_{Bethe} obtained from the Bethe ansatz solution [43] as a function of iteration number, again for a steepest descent (blue dots) and TDVP (green crosses) optimization. In this example, energy minimization converges towards the ground state roughly 100 times faster than TDVP. The difference in performance is even bigger for larger bond dimension D and/or when no lattice optimization is used to initialize the cMPS, in which case TDVP may even fail to converge.

Figure 2(a) illustrates the performance of the proposed energy minimization algorithm as a function of the bond dimension D. For $D = 16$, 32, 64, 128, we computed the reduced energy density $e(\gamma)$ for several values of the dimensionless interaction strength $\gamma \equiv g/\rho$ in the range [0.04, 80] and observed a uniform pattern of convergence towards the exact $e_{\mathrm{Bethe}}(\gamma)$. For reference, a $D = 64$

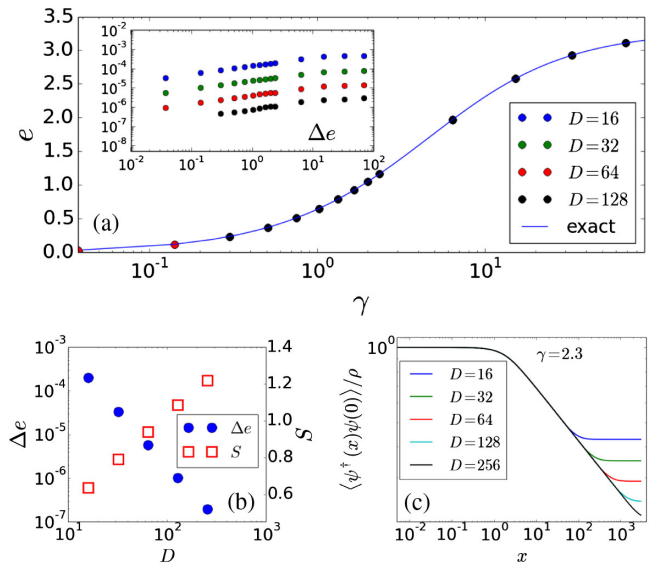

FIG. 2. (a) Reduced energy density e as a function of the dimensionless interaction strength $\gamma \equiv g/\rho$ and cMPS bond dimensions D. The solid line is the exact result from a Bethe ansatz calculation. Data points for different D are on top of each other. The inset shows the error $\Delta e \equiv (e - e_{\mathrm{Bethe}})/e_{\mathrm{Bethe}}$. (b) Relative error Δe in the reduced energy density (filled circles) and bipartite entanglement S (empty squares) of a left-right bipartition, as a function of the bond dimension. (c) Superfluid correlation function, showing saturation to a constant at a finite correlation length ξ, which diverges with growing D.

optimization employing a nonlinear conjugate gradient optimization [28] (stopped once the energy E has converged to 9 digits) takes ∼6 min on a desktop computer [44], including both the lattice initialization (∼2 min) and the nonlinear conjugate gradient optimization in the continuum (∼4 min). This value of the bond dimension is the largest reported so far using TDVP [19,45].

Figures 2(b) and 2(c) specialize to $\gamma \sim 2.3$, $e \sim 1.2$, and consider even larger values of the bond dimensions D, up to 256, to reproduce well-understood finite-D effects of the cMPS representation [45–48]. Figure 2(b) shows the relative error Δe in the reduced energy density and the entanglement entropy $S \equiv -\sum_\alpha (\lambda_\alpha)^2 \log_2(\lambda_\alpha)^2$ across a left-right bipartition, Eq. (6). As expected, Δe vanishes with D as a power law, $\Delta e \sim D^{p_1}$, whereas the entanglement entropy diverges logarithmically, $S \sim \log D$. Figure 2(c) shows the superfluid correlation function $\langle \psi^\dagger(x)\psi(0)\rangle/\rho$, which is seen to saturate to a finite value $|\langle\psi\rangle|^2/\rho$ at some distance ξ, another well-understood artifact of the (c) MPS representation at finite bond dimension D [45–48]. This artificial finite correlation length ξ is seen to diverge with growing D as a power law, $\xi \sim D^{p_2}$.

Once we have established that the optimized cMPS is an accurate approximation to the ground state, we can move to exploring other properties of the model. Figure 3 shows the superfluid correlation function $\langle \psi^\dagger(x)\psi(0)\rangle/\rho$ and pair correlation function $\langle n(x)n(0)\rangle/\rho^2$, respectively, for $D = 128$ and different values of the dimensionless interaction strength γ. With growing γ, we observe an increasingly rapid decay in the superfluid correlation function. The pair correlation function develops typical oscillations that are related to the fermionic nature of the ground state of the Tonks-Girardeau gas [49] at $g = \infty$.

We can also estimate both the central charge c and the Luttinger parameter K, which can be used to uniquely identify the conformal field theory that characterizes the universal low-energy–large-distance features of the model. The central charge c can be estimated from the slope of $S(D)$ (see Ref. [45]). For $\gamma \approx 2.3$ we obtain a value of $c \approx 0.997$, to be compared with the exact value $c = 1$. The Luttinger parameter K [35,50] is obtained from fitting $\log[\langle \psi^\dagger(x)\psi(0)\rangle/\rho]$ versus $\log(x)$ [20], where we choose x to lie in the region where $\langle \psi^\dagger(x)\psi(0)\rangle/\rho$ exhibits power-law decay. For $D = 256$ and $\gamma \approx 2.3$, we obtain

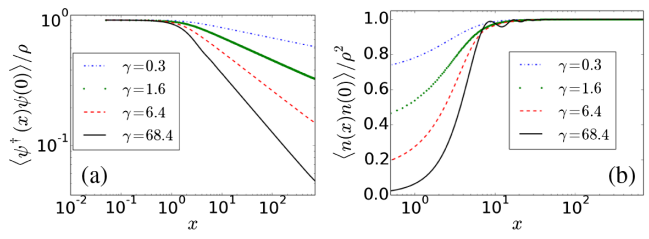

FIG. 3. (a) Superfluid correlation function and (b) pair correlations as a function of the interaction strength γ, for $\mu = -0.5$, $D = 128$.

$K = 2.362 \pm 0.002$. A value of $K = 2.378$ was obtained in Ref. [50] from the weak-coupling approximation of the Bethe ansatz solution. The relative difference to our result is ∼0.7%.

Discussion.—The cMPS is a powerful variational ansatz for strongly interacting quantum field theories in $1+1$ dimensions [16]. In this Letter we have proposed a cMPS energy minimization algorithm with much better performance, in terms of convergence and the attainable bond dimension D, than previous optimization algorithms based on simulating a Euclidean time evolution. For benchmarking purposes, we have applied it to the exactly solvable Lieb-Liniger model, but it performs equally well for a large variety of (nonexactly solvable) field theories [28]. We envisage that this algorithm will play a decisive role in unlocking the full potential of the cMPS representation for ground state studies in the continuum.

Our algorithm works best by initializing the cMPS through an energy optimization on the lattice and by translating the resulting MPS from the lattice to the continuum through Eq. (5). A natural question is then whether the continuum algorithm is needed at all. That is, perhaps—one may wonder—a MPS algorithm working at finite lattice spacing ϵ can already provide a cMPS representation [through Eq. (5)] that can be made arbitrarily close to the one obtained with the continuum algorithm by decreasing ϵ sufficiently. The answer is that this is not possible: lattice algorithms necessarily become unstable as the lattice spacing ϵ is reduced. This can be understood from a simple scaling argument. In discretizing, e.g., the Hamiltonian H of Eq. (15) into a lattice, the nonrelativistic kinetic term $\int \partial_x\psi^\dagger\partial_x\psi$ is seen to diverge with ϵ as $\sim 1/\epsilon^2$, while the rest of the terms in the Hamiltonian have a milder scaling. For small ϵ this creates a large range of energy scales that lead to numerical instability. This effect is compounded with a second fact, revealed by Eq. (5). For small ϵ the MPS matrix $A^0 = \mathbb{1} + \epsilon Q$ is made of two pieces: a constant part $\mathbb{1}$ made of 0's and 1's and the variational parameters ϵQ, which are of order ϵ. Thus, the first part $\mathbb{1}$ shadows the second one, in that the numerical precision on the variational parameters Q is reduced by a factor ϵ when embedded in matrix A^0. The observant reader may then wonder if these problems could be prevented by just changing variables, to work instead with $Q = (A^0 - \mathbb{1})/\epsilon$. This is indeed the case, and also the essence of working with the cMPS representation directly, as we do in the proposed energy minimization algorithm. Notice that lattice MPS techniques can be successfully applied to ground states [51–55] and real-time evolution [56,57] of discretized field theories. However, these simulations are conducted at sufficiently large ϵ and are often plagued with finite ϵ-scaling analysis, which is not necessary when working directly with a cMPS.

We have seen that the cMPS energy minimization algorithm drastically outperforms TDVP at the task of approximating the ground state (we emphasize that the TDVP remains an extremely useful tool, e.g., to simulate

real-time evolution, for which no other method exists). This result did not come as a surprise: on the lattice, MPS energy minimization algorithms, including DMRG, have long been observed to converge to the ground state much faster than time evolution simulation algorithms [5]. We expect the new algorithm to also produce a significant speed-up both for inhomogeneous Hamiltonians [where matrices $Q(x)$ and $R(x)$ depend on space [16,58]] and for a theory of multiple fields $\psi_\alpha(x)$ [18,59–64]), as we will discuss in future work.

The authors thank D. Draxler, V. Zauner-Stauber, A. Milsted, J. Haegeman, F. Verstraete, and E. M. Stoudenmire for useful comments and discussions. The authors also acknowledge support by the Simons Foundation (Many Electron Collaboration). Computations were made on the supercomputer Mammouth parallèle II from University of Sherbrooke, managed by Calcul Québec and Compute Canada. The operation of this supercomputer is funded by the Canada Foundation for Innovation (CFI), the ministère de l'Économie, de la science et de l'innovation du Québec (MESI), and the Fonds de recherche du Québec-Nature et technologies (FRQ-NT). Some earlier computations were conducted at the supercomputer of the Center for Nanophase Materials Sciences, which is a DOE Office of Science User Facility. This research was supported in part by Perimeter Institute for Theoretical Physics. Research at Perimeter Institute is supported by the Government of Canada through Industry Canada and by the Province of Ontario through the Ministry of Economic Development and Innovation.

*martin.ganahl@gmail.com

[1] M. Fannes, B. Nachtergaele, and R. F. Werner, Commun. Math. Phys. **144**, 443 (1992).
[2] S. R. White, Phys. Rev. Lett. **69**, 2863 (1992).
[3] U. Schollwöck, Ann. Phys. (Amsterdam) **326**, 96 (2011).
[4] F. Verstraete, J. I. Cirac, and V. Murg, Adv. Phys. **57**, 143 (2008).
[5] I. P. McCulloch, arXiv:0804.2509.
[6] G. Vidal, Phys. Rev. Lett. **98**, 070201 (2007).
[7] M. B. Hastings, J. Stat. Mech. (2007) P08024.
[8] J. Eisert, M. Cramer, and M. B. Plenio, Rev. Mod. Phys. **82**, 277 (2010).
[9] S. R. White, Phys. Rev. B **48**, 10345 (1993).
[10] G. Vidal, Phys. Rev. Lett. **93**, 040502 (2004).
[11] G. Vidal, Phys. Rev. Lett. **91**, 147902 (2003).
[12] A. J. Daley, C. Kollath, U. Schollwck, and G. Vidal, J. Stat. Mech. (2004) P04005.
[13] S. R. White and A. E. Feiguin, Phys. Rev. Lett. **93**, 076401 (2004).
[14] A. E. Feiguin and S. R. White, Phys. Rev. B **72**, 020404 (2005).
[15] J. Haegeman, J. I. Cirac, T. J. Osborne, I. Pižorn, H. Verschelde, and F. Verstraete, Phys. Rev. Lett. **107**, 070601 (2011).
[16] F. Verstraete and J. I. Cirac, Phys. Rev. Lett. **104**, 190405 (2010).
[17] J. Haegeman, J. I. Cirac, T. J. Osborne, and F. Verstraete, Phys. Rev. B **88**, 085118 (2013).
[18] J. Haegeman, J. I. Cirac, T. J. Osborne, H. Verschelde, and F. Verstraete, Phys. Rev. Lett. **105**, 251601 (2010).
[19] D. Draxler, J. Haegeman, T. J. Osborne, V. Stojevic, L. Vanderstraeten, and F. Verstraete, Phys. Rev. Lett. **111**, 020402 (2013).
[20] J. Rincón, M. Ganahl, and G. Vidal, Phys. Rev. B **92**, 115107 (2015).
[21] D. Draxler, J. Haegeman, F. Verstraete, and M. Rizzi, Phys. Rev. B **95**, 045145 (2017).
[22] In Eq. (5) we neglect other possible matrices, $A^p \equiv (e^{p/2}/p!)R^p$ for $p > 1$, that are not relevant to the current discussion.
[23] E. M. Stoudenmire and S. R. White, Phys. Rev. B **87**, 155137 (2013).
[24] In the limit of an infinite periodic lattice, $L \to \infty$, we can use the Schmidt decomposition of $|\Psi\rangle$ as in Eq. (6), which assumes a lattice with open boundary conditions. Further, in the case of a translation invariant system on an infinite chain, all left-right partitions are equivalent.
[25] J. Haegeman, C. Lubich, I. Oseledets, B. Vandereycken, and F. Verstraete, Phys. Rev. B **94**, 165116 (2016).
[26] L. Vanderstraeten, online lecture notes, http://quantumtensor.pks.mpg.de/index.php/school/.
[27] J. C. Halimeh and V. Zauner-Stauber, arXiv:1610.02019.
[28] See Supplemental Material at http://link.aps.org/supplemental/10.1103/PhysRevLett.118.220402 for a detailed description of the algorithm proposed in the Main Text, including details on initialisation and orthogonalisation procedures for homogeneous continuous Matrix Product States, as well as the nonlinear conjugate gradient extension of our proposed algorithm. We also present additional results for some nonintegrable extensions of the Lieb-Liniger model.
[29] A. Milsted, J. Haegeman, and T. J. Osborne, Phys. Rev. D **88**, 085030 (2013).
[30] E. H. Lieb and W. Liniger, Phys. Rev. **130**, 1605 (1963).
[31] E. H. Lieb, Phys. Rev. **130**, 1616 (1963).
[32] D. Jaksch, C. Bruder, J. I. Cirac, C. W. Gardiner, and P. Zoller, Phys. Rev. Lett. **81**, 3108 (1998).
[33] I. Bloch, Nat. Phys. **1**, 23 (2005).
[34] T. Kinoshita, T. Wenger, and D. S. Weiss, Nature (London) **440**, 900 (2006).
[35] M. A. Cazalilla, R. Citro, T. Giamarchi, E. Orignac, and M. Rigol, Rev. Mod. Phys. **83**, 1405 (2011).
[36] E. Haller, R. Hart, M. J. Mark, J. G. Danzl, L. Reichsollner, M. Gustavsson, M. Dalmonte, G. Pupillo, and H.-C. Nägerls, Nature (London) **466**, 597 (2010).
[37] F. Meinert, M. Knap, E. Kirilov, K. Jag-Lauber, M. B. Zvonarev, E. Demler, and H.-C. Nägerl, arXiv:1608.08200.
[38] S. Prolhac, J. Phys. A **50**, 144001 (2017).
[39] G. Lang, F. Hekking, and A. Minguzzi, arXiv:1609.08865.
[40] Z. Ristivojevic, Phys. Rev. Lett. **113**, 015301 (2014).
[41] M. Zvonarev, Notes on Bethe Ansatz, http://cmt.harvard.edu/demler/TEACHING/Physics284/LectureZvonarev.pdf.
[42] D. Draxler (private communication).
[43] As reference value we take $e_{\mathrm{Bethe}}(\gamma_\infty = g/\rho_\infty)$, where ρ_∞ is the converged particle density at large iteration number of the TDVP or the gradient optimization, respectively.

[44] Run times were measured on a 2014 Intel i7vPro quad core CPU with 8 GB RAM.
[45] V. Stojevic, J. Haegeman, I. P. McCulloch, L. Tagliacozzo, and F. Verstraete, Phys. Rev. B **91**, 035120 (2015).
[46] B. Pirvu, G. Vidal, F. Verstraete, and L. Tagliacozzo, Phys. Rev. B **86**, 075117 (2012).
[47] L. Tagliacozzo, T. R. de Oliveira, S. Iblisdir, and J. I. Latorre, Phys. Rev. B **78**, 024410 (2008).
[48] F. Pollmann, S. Mukerjee, A. M. Turner, and J. E. Moore, Phys. Rev. Lett. **102**, 255701 (2009).
[49] M. Girardeau, J. Math. Phys. (N.Y.) **1**, 516 (1960).
[50] M. A. Cazalilla, J. Phys. B **37**, S1 (2004).
[51] M. Dolfi, B. Bauer, M. Troyer, and Z. Ristivojevic, Phys. Rev. Lett. **109**, 020604 (2012).
[52] E. M. Stoudenmire, L. O. Wagner, S. R. White, and K. Burke, Phys. Rev. Lett. **109**, 056402 (2012).
[53] L. O. Wagner, E. M. Stoudenmire, K. Burke, and S. R. White, Phys. Rev. Lett. **111**, 093003 (2013).
[54] L. O. Wagner, T. E. Baker, E. M. Stoudenmire, K. Burke, and S. R. White, Phys. Rev. B **90**, 045109 (2014).
[55] T. E. Baker, E. M. Stoudenmire, L. O. Wagner, K. Burke, and S. R. White, Phys. Rev. B **91**, 235141 (2015).
[56] M. Knap, C. J. M. Mathy, M. Ganahl, M. B. Zvonarev, and E. Demler, Phys. Rev. Lett. **112**, 015302 (2014).
[57] D. Muth and M. Fleischhauer, Phys. Rev. Lett. **105**, 150403 (2010).
[58] J. Haegeman, D. Draxler, V. Stojevic, J. I. Cirac, T. J. Osborne, and F. Verstraete, arXiv:1501.06575.
[59] F. Quijandría, J. J. García-Ripoll, and D. Zueco, Phys. Rev. B **90**, 235142 (2014).
[60] F. Quijandría and D. Zueco, Phys. Rev. A **92**, 043629 (2015).
[61] S. S. Chung, K. Sun, and C. J. Bolech, Phys. Rev. B **91**, 121108 (2015).
[62] S. S. Chung and C. J. Bolech, arXiv:1612.03149.
[63] D. Draxler, Ph.D. thesis, University of Vienna, 2016.
[64] J. Haegeman, Ph.D. thesis, Ghent University, 2011.